Bandgap control with local and interconnected LC piezoelectric shunts

Author(s):
Flores Parra, Edgar A.; Bergamini, Andrea; Lossouarn, Boris; Van Damme, Bart; Cenedese, Mattia ⓘD; Ermanni, Paolo

Bandgap control with local and interconnected LC piezoelectric shunts

Edgar A. Flores Parra, Andrea Bergamini, Boris Lossouarn, Bart Van Damme, Mattia Cenedese, and Paolo Ermanni

---

Articles you may be interested in

Bandgap control with local and interconnected LC piezoelectric shunts

Edgar A. Flores Parra,[1] Andrea Bergamini,[2,a)] Boris Lossouarn,[3] Bart Van Damme,[4] Mattia Cenedese,[5] and Paolo Ermanni[1]

[1]ETH Zürich, Composite Materials and Adaptive Structures Laboratory, Leonhardstrasse 21, 8092 Zürich, Switzerland
[2]Empa, Laboratory for Mechanical Integrity of Energy Systems, Überlandstrasse 129, 8600 Dübendorf, Switzerland
[3]Cnam, Structural Mechanics and Coupled Systems Laboratory, Rue Saint-Martin 292, 75003 Paris, France
[4]Empa, Laboratory for Acoustics/Noise Control, Überlandstrasse 129, 8600 Dübendorf, Switzerland
[5]Politecnico di Milano, Piazza Leonardo da Vinci 32, 20133 Milano, Italy

This paper reports on the control of longitudinal wave propagation, in the kHz frequency range, using local and interconnected LC (inductance-capacitance) shunts distributed periodically along a rod. The LC shunts are connected to piezoelectric inserts and tuned to engender narrow or broadband pass-bands in the forbidden band frequency range. The Bragg-scattering bandgaps are the result of the periodic mechanical mismatch between PMMA (polymethyl-methacrylate) of the rod and PZT (lead-zirconate-titanate). The narrow pass-bands correspond to the local configuration, where an equivalence between the mechanical impedance of the PMMA and PZT occurs around the shunt resonance frequency. Conversely, the interconnected shunts give a way to an electrical medium through which energy can propagate parallel to its mechanical counterpart, leading to broad pass-bands. This paper presents analytical models for calculating the dispersion and displacements of the 1D medium with interconnected LC shunts. An analytical formulation is also introduced to expediently identify the location of bandgaps and pass-bands in the medium comprised of local LC shunts. Moreover, analytical investigations are carried out to elucidate different physical phenomena giving rise to these pass-bands. The findings are experimentally validated using a finite periodic rod. The ability to tune the dispersion properties of the medium to control the width or depth of the bandgap, by utilizing local or interconnected shunts, offers a new and powerful application for piezoelectric shunts. *Published by AIP Publishing.* [http://dx.doi.org/10.1063/1.4994779]

The community of researchers working on phononic crystals is infusing extensive efforts in controlling the propagation of elastic waves using arrays of shunted piezoelectric elements. Many of the past studies have aimed at reducing structural vibrations through locally shunted piezoelectric elements,[1–3] and to a lesser extent with interconnected piezoelectric shunts.[4,5] This paper reports on a class of 1D phononic crystals, which incorporates local or interconnected arrays of piezoelectric shunts to control longitudinal Bragg-scattering bandgaps by introducing tunable pass-bands. The piezoelectric shunts change the mechanical characteristics of the system, thus allowing for longitudinal waves to propagate in the otherwise forbidden frequency range. This work draws similarity to other investigations, such as the one presented by Thorp *et al.*[6] where piezoelectric patches placed periodically along a rod are tuned to control the location, and width of stop-bands. There is a parallelism with Ruzzene and Baz[7] where a composite rod features periodic inclusions of shape memory alloy (SMA), creating an impedance mismatch for controlling the longitudinal wave transmission. Likewise, there is resemblance to the work by Mansoura *et al.*[8] where the band structure of a piezoelectric phononic crystal is tuned using negative capacitance. Bergamini *et al.* exploited local inductance-capacitance (LC) shunts to introduce a pass-band within a bandgap for transverse mechanical

waves.[9] Khelif *et al.*[10] also reported on two-dimensional phononic crystal where a tunable narrow pass-band is created in a bandgap by varying the geometry of cylindrical inclusions.

In phononic crystals, bandgaps result from discontinuities caused by the periodic mismatch in mechanical impedance, which in turn leads to destructive interference as the incident, reflected, and transmitted waves interact with one another. Due to such interactions, wave propagation is strongly inhibited along a structure[11,12] for wavelengths on the order of the unit-cell size. In metamaterials, on the other hand, the inclusion of suitably designed locally resonating units allows for sub-wavelength modification of the dispersive properties of a medium, as reported among others by Liu in the mechanical domain.[13] While periodicity is not strictly necessary to achieve wave propagation control in correspondence with the tuning frequency of the resonator,[14] it is often assumed to allow for calculating the dispersion properties.

The effect of interconnecting the piezoelectric elements on the dynamic behavior of a structure has been mainly explored by dell'Isola *et al.*[5,15] to control multi-modal vibration damping. In the work by Andreaus *et al.*,[16] a circuit, connecting the piezoelectric elements bonded to the structure, is synthesized analog to the Timoshenko beam. dell'Isola *et al.*[5] optimized an R and LR network to attenuate specific modes, showing that the optimal inductance decreases with the

a)andrea.bergamini@ethz.ch

increasing number of piezoelectric elements. Similar to the latter work, Bergamini *et al.*[17] implemented a network using virtual inductances to attenuate transverse waves in a 1D phononic crystal. Maurini *et al.*[18] performed a more theoretical analysis by comparing the performance of several intricate network topologies acting as vibration absorbers on a beam. Contrary to the previous papers, this contribution focuses on rods as opposed to beams, and the interconnected piezoelectric shunts are aimed at promoting, not attenuating, wave propagation. Furthermore, the PEM (piezoelectromechanical) structures studied in the previous works do not exploit Bragg-scattering bandgaps, as they target frequency vibrations with much longer wavelengths than the unit-cell size.

For the displacement and dispersion studies of both the interconnected and local LC shunt configurations, the rod was made of polymethyl-methacrylate (PMMA) with periodic piezoelectric inserts. PMMA is a viscoelastic material with a complex modulus which varies with frequency and temperature. The complex modulus is almost constant below the glass transition temperature (110 °C).[19] Since the experiments were conducted at room temperature, far below the glass transition temperature, the imaginary/damping component of the modulus was neglected, and a constant Young's modulus, $E_s = 3.3$ GPa, given by the material provider was assumed. The PMMA had a density of $\rho_s = 1190$ kg/m^3, and each PMMA section had a thickness of $l_s = 20$ mm and a cross-section of $A_s = 50$ mm × 30 mm. The piezoelectric material was PIC255, with an open circuit Young's Modulus of $E_p^D = 96$ GPa, a density of $\rho_p = 7800$ kg/m^3, a compliance constant of $s_{33}^E = 2.07 \times 10^{-11}$ m^2/N, a permittivity in the polarization direction of $\epsilon_{33}^T/\epsilon_0 = 1750$, a coupling coefficient of $k_{33} = 0.75$, and a piezoelectric stiffness coefficient of $g = k_{33}\sqrt{E_p^D/(\epsilon_{33}^T/\epsilon_0)(1-k_{33}^2)}$. Each piezoelectric element had a thickness of $l_p = 10$ mm, a cross-section $A_p = A_s$, and a stress-free capacitance of $C_p^\sigma = 2.4$ nF. The subscript s refers to the rod substrate, while the subscript p refers to the insert of the piezoelectric material. The analytical model does not account for material damping. From experimental measurements, each local LC shunt had a resistance of R = 11 Ω, while the whole interconnected line had R = 102 Ω.

The dispersion curves of the phononic crystal are calculated using the transfer matrix method.[20] For both cases, the unit-cell is divided into two continuous regions: PMMA and shunted piezoelectric material (LC local or interconnected) as shown in Figs. 1(a) and 1(b), respectively. For calculating the displacement output at the end of the crystal, u_f, we consider a finite rod made of 9 unit-cells, with a total length of $L_T = 270$ mm. The system was mechanically excited by a unit force applied at one end, and the steady state response at the other end was calculated over the frequency range of interest. For both configurations, the analytical displacement output was extracted from the global displacement vector **U**, calculated from the global stiffness matrix **K$_{global}$**, and global force vector **F$_{global}$**.

The transfer and dynamic stiffness matrices for the locally shunted unit cell, Eqs. (1), (2), (4), and (5), were obtained from the work by Thorp *et al.*[6] The displacement for this configuration was calculated using the dynamic stiffness
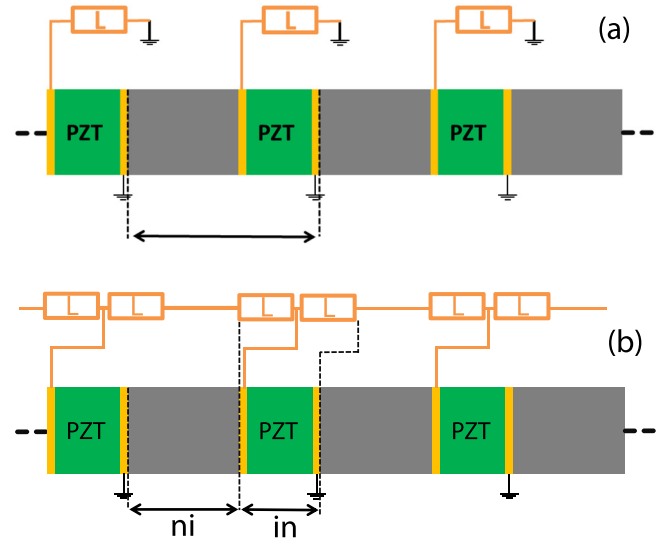

FIG. 1. (a) Unit-cell composed of PMMA and locally shunted piezoelectric element (dotted lines). (b) Unit-cell composed of PMMA, defined as non-interconnected (**ni**), and piezoelectric element with interconnected LC shunts, defined as interconnected (**in**) (dotted lines).

matrices of the two regions of the unit-cell, given by Eqs. (1) and (2), respectively. It is paramount to note that the analytical Bragg-scattering bandgap, Figs. 2(b), 3, and 4(c), begins around 14 kHz, while the experimental one shown in Figs. 2(d) and 4(d) starts around 16 kHz. This discrepancy can be explained by the fact that the analytical models hereby presented (local, interconnected, and the modified characteristic equation for identifying bandgaps) account for purely longitudinal and not transverse deformations.

$$\mathbf{K_s}(\omega) = \frac{E_s A_s k_s}{\sin(k_s l_s)}\begin{bmatrix} \cos(k_s l_s) & -1 \\ -1 & \cos(k_s l_s) \end{bmatrix}, \quad (1)$$
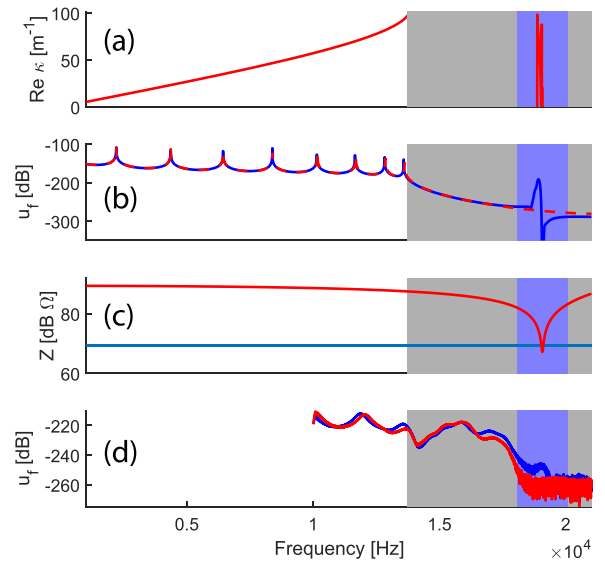
FIG. 2. Gray shading and blue shading correspond to bandgap and pass-band frequency regions, respectively. (a) Dispersion of the locally shunted configuration. (b) Analytical displacement output for the locally shunted configuration (blue) and for the purely mechanical system (red). (c) Mechanical impedance of PMMA (blue) and frequency dependent mechanical impedance of shunted PZT (red). (d) Experimental displacement output for the locally shunted configuration (blue) and for the purely mechanical system (red).

FIG. 3. Analytical bandgap and pass-band indicator for the local LC shunted configuration, where the dotted line represents the right hand side of Eq. (7). Gray shading and blue shading correspond to bandgap and pass-band frequency regions, respectively.

where the substrate wavenumber is $k_s(\omega) = \omega\sqrt{\rho_s/E_s}$, with ω being the angular frequency.

$$\mathbf{K_p}(\omega) = \frac{E_p A_p k_p}{\sin(k_p l_p)}\begin{bmatrix} \cos(k_p l_p) & -1 \\ -1 & \cos(k_p l_p) \end{bmatrix}, \quad (2)$$
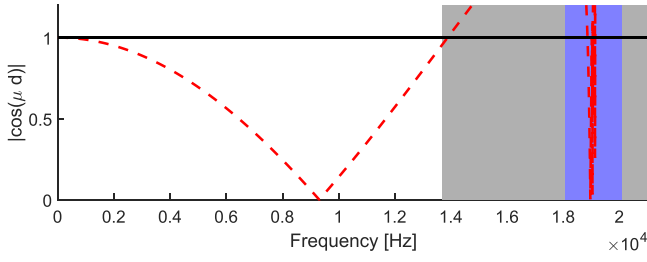
where the lead-zirconate-titanate (PZT) wavenumber is $k_p(\omega) = \omega\sqrt{\rho_p/E_p(\omega)}$ and the complex Young's modulus is as follows:[21]

$$E_p(\omega) = \frac{i\omega R - \omega^2 L + 1/C_p^\sigma}{(S_{33} - d_{33}^2/\epsilon_{33})(i\omega R - \omega^2 L) + S_{33}/C_p^\sigma}. \quad (3)$$

Note that Eq. (3), a formulation for the equivalent Young's modulus of the piezoelectric material, is only valid when considering a sufficiently large wavelength compared to the size of the piezoelectric insert.[22] In this work, the condition satisfied because as we restrain the analysis to the first bandgap, i.e., half a wavelength of the unit-cell.

The transfer matrices for the two regions of the unit-cell are given by Eqs. (4) and (5). The complete unit-cell transfer matrix is assembled according to Eq. (6).
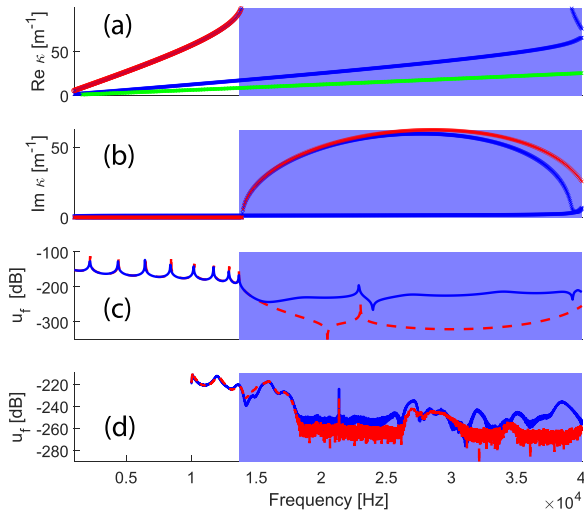

FIG. 4. Blue shading corresponding to the pass-band frequency region. (a) Dispersion of the interconnected configuration [coupled modes (blue)] and dispersion of the purely electrical mode [LC transmission line (green)] and purely mechanical system (red). (b) Imaginary dispersion of the interconnected configuration [coupled modes (blue)] and imaginary dispersion of the purely mechanical system (red). (c) Analytical displacement output for the interconnected configuration (blue) and for the purely mechanical system (red). (d) Experimental displacement output for the interconnected configuration (blue) and for the purely mechanical system (red).

$$\mathbf{T_s}(\omega) = \begin{bmatrix} \cos(k_s l_s) & -\dfrac{\sin(k_s l_s)}{z_s \omega} \\ z_s \omega \sin(k_s l_s) & \cos(k_s l_s) \end{bmatrix}, \quad (4)$$

where the substrate mechanical impedance is $z_s = A_s\sqrt{E_s \rho_s}$

$$\mathbf{T_p}(\omega) = \begin{bmatrix} \cos(k_p l_p) & -\dfrac{\sin(k_p l_p)}{z_p \omega} \\ z_p \omega \sin(k_p l_p) & \cos(k_p l_p) \end{bmatrix}, \quad (5)$$

where the PZT mechanical impedance is $z_p(\omega) = A_p\sqrt{E_p(\omega)\rho_p}$

$$\mathbf{T_{cell}}(\omega) = \mathbf{T_p T_s}. \quad (6)$$

In the work on periodic composite rods by Ruzzene and Baz,[7] an analytical formulation, Eq. (7), was derived to identify the bandgap frequency ranges in periodically inhomogeneous rods.

$$\cos(\mu d) = \cos(k_s l_s)\cos(k_p l_p) - \frac{1}{2}\left(\frac{z_s}{z_p} + \frac{z_p}{z_s}\right)\sin(k_s l_s)\sin(k_p l_p). \quad (7)$$

Modifying this formulation to account for the local LC shunts, the location of the bandgaps and pass-bands can be expediently determined. In Eq. (7), the wavenumber and mechanical impedance are given by $k_i = \omega\sqrt{\rho_i/E_i}$ and $z_i = k_i E_i$ with $i = \{s, p\}$, where $d = l_s + l_p$ is the unit-cell length and μ is the propagation constant that quantifies the nature of the wave traveling along the rod. In the case under study, the locally shunted piezoelectric material is characterized by a frequency dependent Young's modulus, $E_p(\omega)$. According to Eq. (7), bandgaps correspond to the frequencies where $|\cos(\mu d)| > 1$, i.e., μ is complex, while the pass-band regions are defined by $|\cos(\mu d)| \leq 1$, i.e., μ is real. This can be seen in Fig. 3, where the curve of $|\cos(\mu d)|$ goes above one over the expected bandgap range, except at the coincidence frequency, $f_c = 1/\left(2\pi\sqrt{LC_p^\sigma}\right)$, where the curve drops below one, indicating the presence of a pass-band.

As seen in the dispersion curves of Fig. 2(a), the zero-group velocity mode characteristic of the local LC shunts can be seen within the bandgap. The displacement curves in Fig. 2(b) show that the local LC shunts engender a narrow pass-band within the mechanical Bragg-scattering bandgap. This pass-band can be explained by the occurrence of homogeneous mechanical impedance along the length of the rod at f_c, where the variation in the Young's modulus of piezoelectric element yields an equivalence in the mechanical impedance of the two materials, as shown in Fig. 2(c).

The experimental setup, seen in Fig. 5, did not change for both configurations. PMMA and PZT were glued together using low viscosity super-glue, while conducting copper tape was placed between each section to facilitate connecting to the electrodes. Inductances were placed on a breadboard to facilitate switching between the two configurations; $L = 30\,\text{mH}$ was used for the local configuration, while $L = 15\,\text{mH}$ was used for the interconnected. The
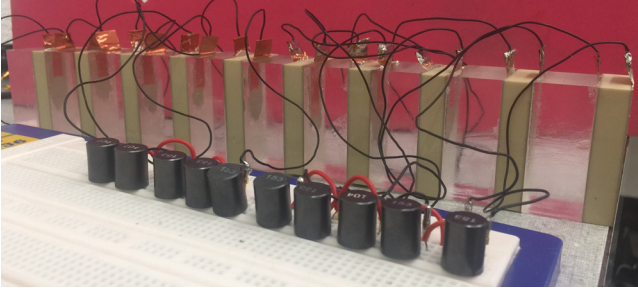
FIG. 5. Experimental setup for local and interconnected shunts.

sample was excited using the first piezoelectric element, powered by a high voltage amplifier from 10 kHz to 40 kHz. This experimental frequency range was chosen based on the limits of the amplifier and the location of the bandgap. A laser vibrometer measured the output displacement on the opposite end of the sample.

The transfer and dynamic stiffness matrices for the interconnected unit-cell presented in this section were derived following the procedure described by Belloni *et al.*[23] The dynamic stiffness matrix of the interconnected region is given by

$$\mathbf{K_{in}}(\omega) = \begin{bmatrix} [\mathbf{A}] & [\mathbf{B}] \\ [\mathbf{B}] & [\mathbf{A}] \end{bmatrix}, \tag{8}$$

where the components of the symmetric $\mathbf{K_{in}}$ matrix are

$$\mathbf{A} = \begin{bmatrix} E^D A_p k_p \dfrac{\cos(k_p l_p)}{\sin(k_p l_p)} & -g \\ -g & \dfrac{1 - \omega^2 (L/2) C_p^\epsilon + i\omega R C_p^\epsilon}{C_p^\epsilon} \end{bmatrix},$$

$$\mathbf{B} = \begin{bmatrix} -E^D A_p k_p \dfrac{1}{\sin(k_p l_p)} & g \\ g & -\dfrac{1}{C_p^\epsilon} \end{bmatrix}.$$

The transfer matrix of the interconnected region of the unit-cell can be obtained from the below equation:

$$\mathbf{T_{in}}(\omega) = \begin{bmatrix} -\mathbf{B}^{-1}\mathbf{A} & \mathbf{B}^{-1} \\ \mathbf{A}\mathbf{B}^{-1}\mathbf{A} - \mathbf{B} & -\mathbf{A}\mathbf{B}^{-1} \end{bmatrix}. \tag{9}$$

The transfer matrix for the non-interconnected region of the unit-cell is given by

$$\mathbf{T_{ni}}(\omega) = \begin{bmatrix} \cos(k_s l_s) & 0 & -\dfrac{\sin(k_s l_s)}{E_s A_s k_s} & 0 \\ 0 & 1 & 0 & 0 \\ E_s A_s k_s \sin(k_s l_s) & 0 & \cos(k_s l_s) & 0 \\ 0 & 0 & 0 & 1 \end{bmatrix}. \tag{10}$$

The last step is the assembly of the complete unit-cell transfer matrix.

$$\mathbf{T_{cell}}(\omega) = \begin{bmatrix} \mathbf{T}_{11} & \mathbf{T}_{12} \\ \mathbf{T}_{21} & \mathbf{T}_{22} \end{bmatrix} = \mathbf{T_{in}}\mathbf{T_{ni}}. \tag{11}$$

The dynamic stiffness matrix of the interconnected unit-cell can be obtained from the below equation:

$$\mathbf{K_{cell}}(\omega) = \begin{bmatrix} -\mathbf{T}_{12}^{-1}\mathbf{T}_{11} & \mathbf{T}_{12}^{-1} \\ \mathbf{T}_{22}\mathbf{T}_{12}^{-1}\mathbf{T}_{11} - \mathbf{T}_{21} & -\mathbf{T}_{22}\mathbf{T}_{12}^{-1} \end{bmatrix}. \tag{12}$$

The interconnections form a discrete transmission line, an electrical medium through which energy can propagate parallel to the mechanical medium. It is paramount to note that the modes of the coupled electrical and mechanical media can no longer be considered purely electrical nor mechanical but rather electromechanical. As seen in Fig. 4(a), the shape of the coupled electromechanical modes is similar to that of their uncoupled counterparts, and thus, we will refer to them as "pseudo" modes. Figure 4(a) shows the dispersion curves of this configuration, where the pseudo-electrical mode is tuned to cross into the frequency range of the mechanical bandgap. As a result, energy can propagate along the electrical medium and back into the mechanical over the forbidden frequency range, thus "disabling" the bandgap. The latter is illustrated in Fig. 4(c), with the analytical velocity over force transmittance curves of the purely mechanical system compared to the coupled system. The analytical results are experimentally validated in Fig. 4(d), where a finite sample was tested with and without the interconnected shunts. The mechanism that allows mechanical waves to propagate in the region of the bandgap is further elucidated by Fig. 4(b), which shows the imaginary dispersion curves for the purely mechanical system (red) and the coupled system (blue). Wavenumbers can be real, imaginary, or complex, representing propagating, evanescent, and attenuating oscillatory waves, respectively.[24] Figure 4(b) illustrates that for the purely mechanical system, there exists a true bandgap wave when Im $\{k_{mech}\} \neq 0$. However, in the case of the coupled system, there are two imaginary electromechanical modes over the frequency range corresponding to the purely mechanical bandgap. These two modes are characterized by the following imaginary wavenumbers: Im $\{k_{pseudomech}\} \neq 0$ and Im $\{k_{pseudoelec,}\} = 0$. These results suggest the existence of attenuating and propagating waves, which results in "disabling" of the purely mechanical Bragg-scattering bandgap of Figs. 4(c) and 4(d).

We have shown that local and interconnected LC piezoelectric shunts can be tuned to give a way to pass-bands of varying frequency ranges. The frequency dependent Young's modulus of local LC shunts can be exploited to transform the phononic crystal, of periodic mismatching mechanical impedances, into a homogeneous medium for wave propagation. This variation in the Young's modulus occurs close to the LC resonance frequency, and thus, the impedance match between the two periodic materials occurs over a narrow frequency range. Conversely, the interconnected configuration utilizes a different mechanism, whereby the LC shunts form a discrete electrical transmission line through which waves can propagate parallel to the mechanical medium, effectively "disabling" the Bragg-scattering bandgap. The mechanism

for the interconnected configuration can be explained by studying the imaginary dispersion curves. The coupled mechanical and electrical media give a way to electromechanical modes which exhibit a combination of propagating and attenuating waves.

[1]J. J. Hollkamp, J. Intell. Mater. Syst. Struct. **5**, 49 (1994).

[2]B. S. Beck, K. A. Cunefare, M. Ruzzene, and M. Collet, J. Intell. Mater. Syst. Struct. **22**, 1177 (2011).

[3]A. Spadoni, M. Ruzzene, and K. Cunefare, J. Intell. Mater. Syst. Struct. **20**, 979 (2009).

[4]B. Lossouarn, M. Aucejo, and J. Deü, Smart Mater. Struct. **24**, 045018 (2015).

[5]F. dell'Isola, C. Maurini, and M. Porfiri, Smart Mater. Struct. **13**, 299 (2004).

[6]O. Thorp, M. Ruzzene, and A. Baz, Smart Mater. Struct. **10**, 979 (2001).

[7]M. Ruzzene and A. Baz, Trans.-ASME J. Vib. Acoust. **122**, 151 (2000).

[8]S. A. Mansoura, B. Morvan, P. Maréchal, P. Benard, A.-C. Lhadky-Hennion, and B. Dubus, in *2015 IEEE International Ultrasonics Symposium (IUS)* (IEEE, 2015), pp. 1–4.

[9]A. Bergamini, T. Delpero, L. D. Simoni, L. D. Lillo, M. Ruzzene, and P. Ermanni, Adv. Mater. **26**, 1343 (2014).

[10]A. Khelif, P. Deymier, B. Djafari-Rouhani, J. Vasseur, and L. Dobrzynski, J. Appl. Phys. **94**, 1308 (2003).

[11]L. Brillouin, *Wave Propagation in Periodic Structures: Electric Filters and Crystal Lattices* (Courier Corporation, 1946).

[12]P. A. Deymier, *Acoustic Metamaterials and Phononic Crystals* (Springer Science & Business Media, 2013), Vol. 173.

[13]Z. Liu, X. Zhang, Y. Mao, Y. Zhu, Z. Yang, C. Chan, and P. Sheng, Science **289**, 1734 (2000).

[14]H. Huang and C. Sun, Philos. Mag. **91**, 981 (2011).

[15]R. C. Batra, F. dell'Isola, S. Vidoli, and D. Vigilante, Int. J. Solids Struct. **42**, 3115 (2005).

[16]U. Andreaus, F. DellIsola, and M. Porfiri, Modal Anal. **10**, 625 (2004).

[17]A. E. Bergamini, M. Zündel, E. A. F. Parra, T. Delpero, M. Ruzzene, and P. Ermanni, J. Appl. Phys. **118**, 154310 (2015).

[18]C. Maurini, F. dell'Isola, and D. Del Vescovo, Mech. Syst. Signal Process. **18**, 1243 (2004).

[19]G. Cheng, J. C. Gelin, and T. Barrière, in *Key Engineering Materials* (Trans Tech Publications, 2013), Vol. 554, pp. 1763–1776.

[20]L. Airoldi, M. Senesi, and M. Ruzzene, in *Wave Propagation in Linear and Nonlinear Periodic Media* (Springer, 2012), pp. 33–108.

[21]N. W. Hagood and A. von Flotow, J. Sound Vib. **146**, 243 (1991).

[22]C. Shengbing, W. Jihong, W. Gang, Y. Dianlong, and W. Xisen, J. Intell. Mater. Syst. Struct. **23**, 1613 (2012).

[23]E. Belloni, M. Cenedese, and F. Braghin, in *SPIE Smart Structures and Materials+ Nondestructive Evaluation and Health Monitoring* (International Society for Optics and Photonics, 2017), pp. 101642Y–101642Y.

[24]B. R. Mace and E. Manconi, J. Acoust. Soc. Am. **131**, 1015 (2012).